Cell Reports
Article

GPR56/ADGRG1 Inhibits Mesenchymal Differentiation and Radioresistance in Glioblastoma

Marta Moreno,[1] Leire Pedrosa,[1,2] Laia Paré,[2] Estela Pineda,[2,3] Leire Bejarano,[1] Josefina Martínez,[7] Veerakumar Balasubramaniyan,[8] Ravesanker Ezhilarasan,[9] Naveen Kallarackal,[9] Sung-Hak Kim,[10] Jia Wang,[10] Alessandra Audia,[11] Siobhan Conroy,[12] Mercedes Marin,[2] Teresa Ribalta,[4,19] Teresa Pujol,[5] Antoni Herreros,[6] Avelina Tortosa,[7] Helena Mira,[13] Marta M. Alonso,[14,15,16] Candelaria Gómez-Manzano,[8] Francesc Graus,[17] Erik P. Sulman,[9] Xianhua Piao,[18] Ichiro Nakano,[10] Aleix Prat,[1,2,3] Krishna P. Bhat,[11] and Núria de la Iglesia[1,2,20,*]
[1]Glioma and Neural Stem Cell Group
[2]Translational Genomics and Targeted Therapeutics in Solid Tumors Team
August Pi i Sunyer Biomedical Research Institute (IDIBAPS), Barcelona, Spain
[3]Department of Medical Oncology
[4]Department of Pathology
[5]Department of Radiology
[6]Department of Radiation Oncology
Hospital Clinic, Barcelona, Spain
[7]Department of Basic Nursing, Universitat de Barcelona-Institut d'Investigació Biomèdica de Bellvitge (IDIBELL), Barcelona, Spain
[8]Department of Neuro-Oncology
[9]Department of Radiation Oncology
The University of Texas, M.D. Anderson Cancer Center, Houston, TX 77030, USA
[10]Department of Neurosurgery, Comprehensive Cancer Center, University of Alabama at Birmingham, AL 35233, USA
[11]Department of Translational Molecular Pathology, The University of Texas, M.D. Anderson Cancer Center, Houston, TX 77030, USA
[12]Department of Pathology and Medical Biology, University Medical Center Groningen, Groningen, the Netherlands
[13]Stem Cells and Aging Unit, Biomedicine Institute of València (IBV), Spanish National Research Council (CSIC), València, Spain
[14]Department of Pediatrics, University Hospital of Navarra, Pamplona, Navarra, Spain
[15]The Health Research Institute of Navarra (IDISNA), Pamplona, Spain
[16]Program in Solid Tumors and Biomarkers, Foundation for Applied Medical Research (CIMA), Pamplona, Spain
[17]Clinical and Experimental Neuroimmunology, IDIBAPS, Barcelona, Spain
[18]Division of Newborn Medicine, Department of Medicine, Boston Children's Hospital and Harvard Medical School, Boston, MA 02115, USA
[19]Human and Experimental Functional Oncomorphology, IDIBAPS, Barcelona, Spain
[20]Lead Contact
*Correspondence: niglesia@clinic.cat
https://doi.org/10.1016/j.celrep.2017.10.083

SUMMARY

A mesenchymal transition occurs both during the natural evolution of glioblastoma (GBM) and in response to therapy. Here, we report that the adhesion G-protein-coupled receptor, GPR56/ADGRG1, inhibits GBM mesenchymal differentiation and radioresistance. GPR56 is enriched in proneural and classical GBMs and is lost during their transition toward a mesenchymal subtype. GPR56 loss of function promotes mesenchymal differentiation and radioresistance of glioma initiating cells both *in vitro* and *in vivo*. Accordingly, a low GPR56-associated signature is prognostic of a poor outcome in GBM patients even within non-G-CIMP GBMs. Mechanistically, we reveal GPR56 as an inhibitor of the nuclear factor kappa B (NF-κB) signaling pathway, thereby providing the rationale by which this receptor prevents mesenchymal differentiation and radioresistance. A pan-cancer analysis suggests that GPR56 might be an inhibitor of the mesenchymal transition across multiple tumor types beyond GBM.

INTRODUCTION

Glioblastomas (GBMs) are the most frequent and aggressive primary tumors in the central nervous system owing to their fast clinical course and uniform lethality (Dunn et al., 2012; Louis et al., 2016). Adult GBMs can be classified according to their gene expression and epigenetic profiles into five different subtypes as follows: glioma-CpG island methylator phenotype (G-CIMP) and four non-G-CIMP subtypes termed proneural (PN), neural, classical (CL), and mesenchymal (MES) (Brennan et al., 2013; Noushmehr et al., 2010; Verhaak et al., 2010). G-CIMP GBMs are tightly associated with somatic mutations in the IDH1 or IDH2 genes (Parsons et al., 2008; Yan et al., 2009) and show a more favorable prognosis, whereas non-G-CIMP GBM patients have the poorest prognosis (Noushmehr et al., 2010) with the MES subtype correlating with higher radioresistance and shorter survival (Bhat et al., 2013; Patel et al., 2014).

Non-G-CIMP GBMs display elevated transcriptional plasticity and have an intrinsic ability to transition from one subtype to another. The best characterized of these transitions is the PN-to-MES transition (PMT), which is associated with tumor recurrence (Phillips et al., 2006) and acquired resistance to anti-angiogenic therapy (Piao et al., 2013). Along the same lines,

non-G-CIMP GBMs, including MES-GBMs, have been proposed to evolve from a common PN-like precursor glioma during GBM evolution (Ozawa et al., 2014). Analogous to whole tumors, isolated tumor cell cultures that are enriched in glioma stem-like initiating cells (GICs) also display the GBM-subtype-specific phenotypes (Bhat et al., 2013; Mao et al., 2013; Patel et al., 2014; Xie et al., 2015). Nonetheless, GICs are highly plastic and also undergo transitions from PN to MES identity, especially in response to inflammation or ionizing radiation (Bhat et al., 2013; Halliday et al., 2014; Mao et al., 2013; Segerman et al., 2016). Although we and others have identified some of the molecular mediators that promote MES differentiation, such as nuclear factor kappa B (NF-κB) (Bhat et al., 2013), the negative modulators of this process remain unknown. Deciphering the molecular mechanisms that control MES differentiation is of crucial interest to understand both GBM natural evolution as well as acquired resistance to therapy.

The acquisition of a MES phenotype in GBM has been linked to the activation of master transcription factors and co-factors that control an epithelial-to-mesenchymal transition (EMT) such as STAT3, C/EBPβ, and TAZ (Bhat et al., 2011; Bundy and Sealy, 2003; Carro et al., 2010; Chen et al., 2014; Lei et al., 2008; Lo et al., 2007; Xiong et al., 2012). During EMT, either in embryonic development or in tumorigenesis, epithelial cells lose polarity, reduce cellular adhesion, and increase cell migration (Mani et al., 2008; Thiery et al., 2009). In a large number of systems, the loss of cell adhesion that is required to initiate EMT is achieved through the repression of the epithelial marker E-cadherin, which is a transmembrane calcium-dependent glycoprotein that is responsible for cell-to-cell adhesion. However, limited expression of E-cadherin in normal brain tissue and GBMs suggests that other adhesion proteins might be playing a role in this process (Lewis-Tuffin et al., 2010).

Adhesion G-protein-coupled receptors (GPCRs), which are an atypical class of GPCRs, are characterized by an unusually long extracellular domain that is involved in cell-to-cell and cell-to-extracellular matrix interactions (Langenhan et al., 2013). Several adhesion-GPCRs, including GPR56/ADGRG1, are highly expressed in the brain. In the present study, we investigated the role of GPR56 in GBM pathogenesis by integrating the analysis of clinical specimens with functional assays in GICs and identified the role of GPR56 as an inhibitor of MES differentiation. GPR56 knockdown promotes MES differentiation of GICs, which is accompanied by increased radioresistance both *in vitro* and *in vivo*. Accordingly, a low GPR56-associated signature is prognostic of a poor outcome in non-G-CIMP GBM patients. Furthermore, we identified GPR56 as an inhibitor of the NF-κB signaling pathway, and pan-cancer analyses suggested that this receptor might have an analogous function in other cancer types beyond GBM.

RESULTS

GPR56 Is Downregulated in MES-GBMs and Inversely Correlated with MES Markers in GBM Specimens

To identify inhibitors of MES differentiation in GBMs, we searched within the class of adhesion-GPCRs for receptors that are differentially expressed across GBM subtypes. We reasoned that potential inhibitors of MES differentiation would be downregulated in MES-GBMs with respect to other subtypes. We analyzed mRNA expression of the 33 adhesion-GPCR members in GBM specimens from The Cancer Genome Atlas (TCGA) dataset (Brennan et al., 2013). A group-comparison analysis between the five different GBM subtypes revealed the downregulation of four adhesion-GPCRs in MES-GBMs versus the rest of GBM subtypes: *GPR56*, *BAI1*, *BAI3*, and *CELSR3* (Figures 1A and S1). Among these, GPR56 emerged as a promising candidate since its biological functions in the context of a normal brain pointed to a possible role in counteracting an EMT-like process. This receptor serves as an extracellular matrix receptor that mediates the attachment of radial glial progenitors to the pial basement membrane (Li et al., 2008), while it inhibits the migration of neural progenitors and invasion and metastasis in other tumor types, especially melanoma (Luo et al., 2011; Xu et al., 2006, 2010). Furthermore, GPR56 has a crucial role in brain development (Bae et al., 2014; Piao et al., 2004) and is highly expressed in neural stem cells (NSCs) and oligodendrocyte progenitor cells (OPCs) (Ackerman et al., 2015; Giera et al., 2015; Jeong et al., 2012), which are two proposed cells of origin of GBM (Alcantara Llaguno et al., 2015; Liu et al., 2011).

We next analyzed the correlation between *GPR56* expression and published PN or MES signatures (Verhaak et al., 2010). As expected, *GPR56* mRNA levels were positively and negatively correlated with PN and MES signatures, respectively (Figure 1B). To validate our above analyses using the TCGA dataset (Figures 1A and 1B), we examined the expression of GPR56 along with MES markers via immunohistochemistry in an independent cohort of human GBM specimens (Ohio State University dataset [Mao et al., 2013]). In this cohort, samples with a high expression of GPR56 had lower levels of ALDH1A3, a well-established MES marker (Mao et al., 2013). Conversely, GBMs with a low expression of GPR56 were highly immunoreactive for ALDH1A3 (Figure 1C). Interestingly, GPR56 is downregulated in recurrent GBMs (Figure 1D), which, in many cases, have undergone a shift toward an MES subtype (Phillips et al., 2006; Wang et al., 2016, 2017). Taken together, our results imply that GPR56 negatively correlates with the MES subtype and may be downregulated during MES differentiation in GBMs.

GPR56 Is Highly Expressed in PN-GICs and Downregulated during Their MES Transition in Response to TNF-α

We next analyzed whether GICs show similar patterns of GPR56 expression to those observed in clinical specimens. We compared the levels of *GPR56* mRNA in PN- versus MES-GIC lines in the following two independent datasets: GEO: GSE49009 (Bhat et al., 2013) and GEO: GSE67089 (Mao et al., 2013). GEO: GSE49009 contains 11 PN-GICs and 6 MES-GICs. GEO: GSE67089 contains 6 PN-GICs and 4 MES-GICs. In both datasets, we observed that GPR56 mRNA levels were significantly higher in PN-GICs than in MES-GICs (Figure 2A).

To further study the differential expression of GPR56 in PN versus MES subtypes, we sorted GIC lines into $CD44^{high}$ and $CD44^{low}$ subpopulations (Figure S2A), which have previously been shown to be enriched in MES and PN subtypes,

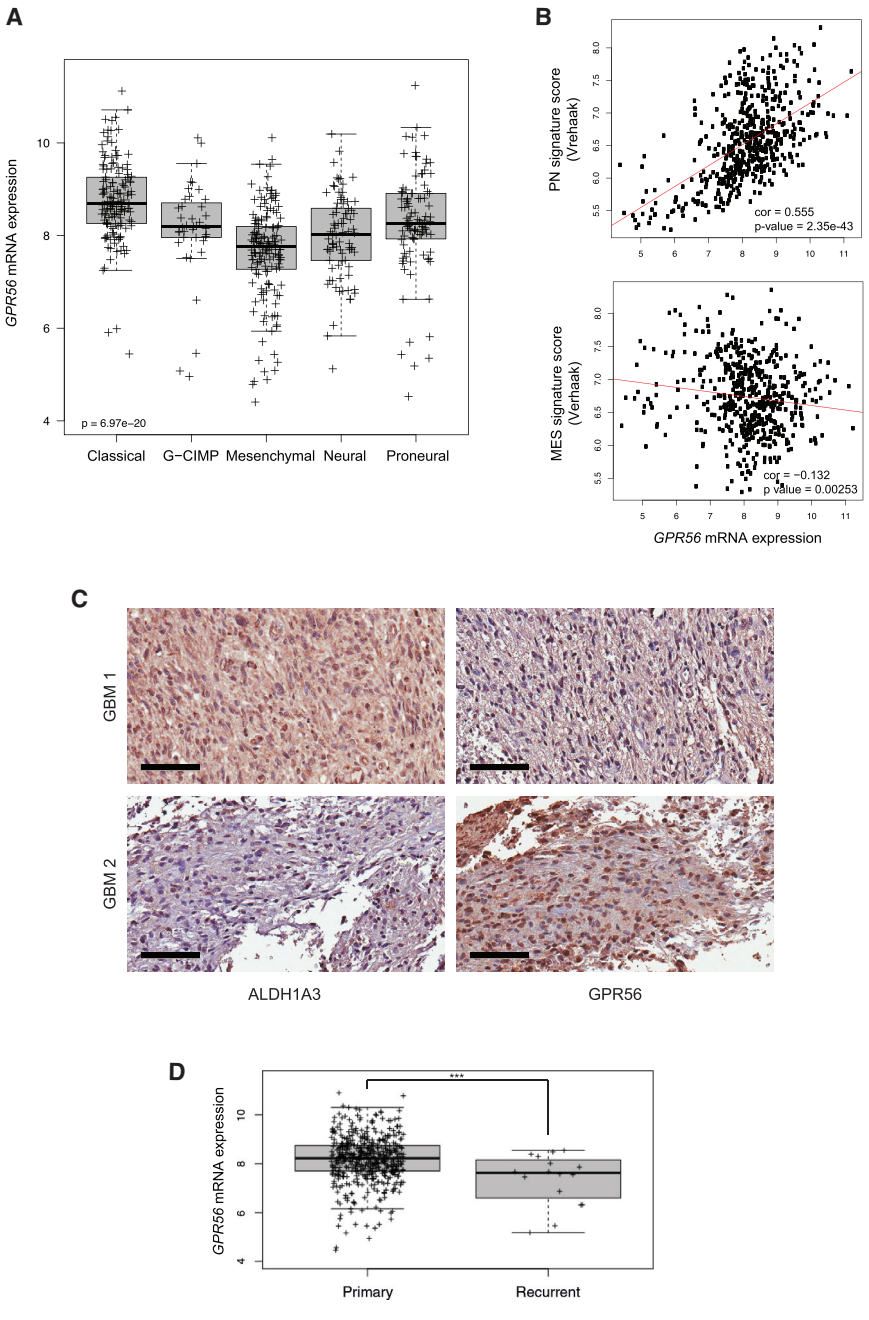

Figure 1. GPR56 Is Downregulated in MES-GBMs and Inversely Correlated with MES Markers

(A) *GPR56* mRNA expression comparison across the five different subtypes of GBM (TCGA dataset). Gene expression data were obtained from Brennan et al. (2013) (Table S1). Differences in *GPR56* expression among subtypes were assessed by a Kruskal-Wallis rank-sum test (Dunn's post hoc multiple comparison test: MES versus classical and proneural, $p < 0.0001$; MES versus G-CIMP, $p < 0.001$; MES versus neural, $p < 0.01$). In the box-plots, the horizontal line indicates the median, boundaries of the box indicate the first and third quartiles, and whiskers indicate confidence intervals (95%). See also Figure S1 and Table S1.

(B) Correlation plots between *GPR56* mRNA levels and proneural (upper panel) or mesenchymal (lower panel) signature scores in GBM patients from the TCGA dataset. Pearson's correlation coefficients and p values are indicated in each plot.

(C) Immunohistochemistry of GPR56 and the MES marker ALDH1A3 in two representative paraffin-embedded human GBM specimens from the Ohio State University cohort (n = 24). Scale bar, 80 μm.

(D) *GPR56* mRNA expression comparison between primary and recurrent GBMs (TCGA dataset). Differences in *GPR56* expression were assessed by Kruskal-Wallis rank sum test (Dunn's post hoc multiple comparison test: primary versus recurrent, ***$p = 0.002$). In the box-plots, the horizontal line indicates the median, boundaries of the box indicate the first and third quartiles, and whiskers indicate confidence intervals (95%).

respectively (Bhat et al., 2013; Mao et al., 2013), and analyzed the expression levels of GPR56 in these cells. An RT-qPCR and western blot analysis revealed that GPR56 was weakly expressed in CD44^{high} GICs, whereas it was highly enriched in CD44^{low} GICs (Figures 2B and 2C). Furthermore, we obtained similar results using ALDH1A3, which is another MES-GBM marker (Mao et al., 2013). *GPR56* mRNA expression was low in ALDH1A3^{high} GICs, while it was upregulated in ALDH1A3^{low} GICs (Figures 2D and S2B).

The pro-inflammatory cytokine tumor necrosis factor alpha (TNF-α) has been shown to induce MES differentiation in GICs (Bhat et al., 2013). Because GPR56 is poorly expressed in MES-GICs, we next asked whether TNF-α treatment downregulates GPR56 expression in PN-GICs. Indeed, TNF-α promoted a decrease in *GPR56* mRNA expression in all of the PN-GIC lines tested (Figures 2E and S2C) while increasing *CD44* mRNA expression (Figure 2E). Moreover, TNF-α promoted a decrease in GPR56 protein levels in CD44^{low} cells (Figure 2F). Taken together, our results show that GPR56 expression is inversely correlated with a MES phenotype both in GICs and GBM specimens and that GPR56 is downregulated during TNF-α-mediated MES differentiation.

Loss of GPR56 Promotes MES Differentiation *In Vitro* and *In Vivo*

Given our observations that GPR56 is downregulated during the MES differentiation of PN-GICs, we asked whether GPR56 is functionally involved in this process. To test our hypothesis, we examined whether GPR56 downregulation is required for CD44 expression by loss-of-function studies in PN-GICs. To this end, we first used short-hairpin-RNA (shRNA)-mediated knockdown

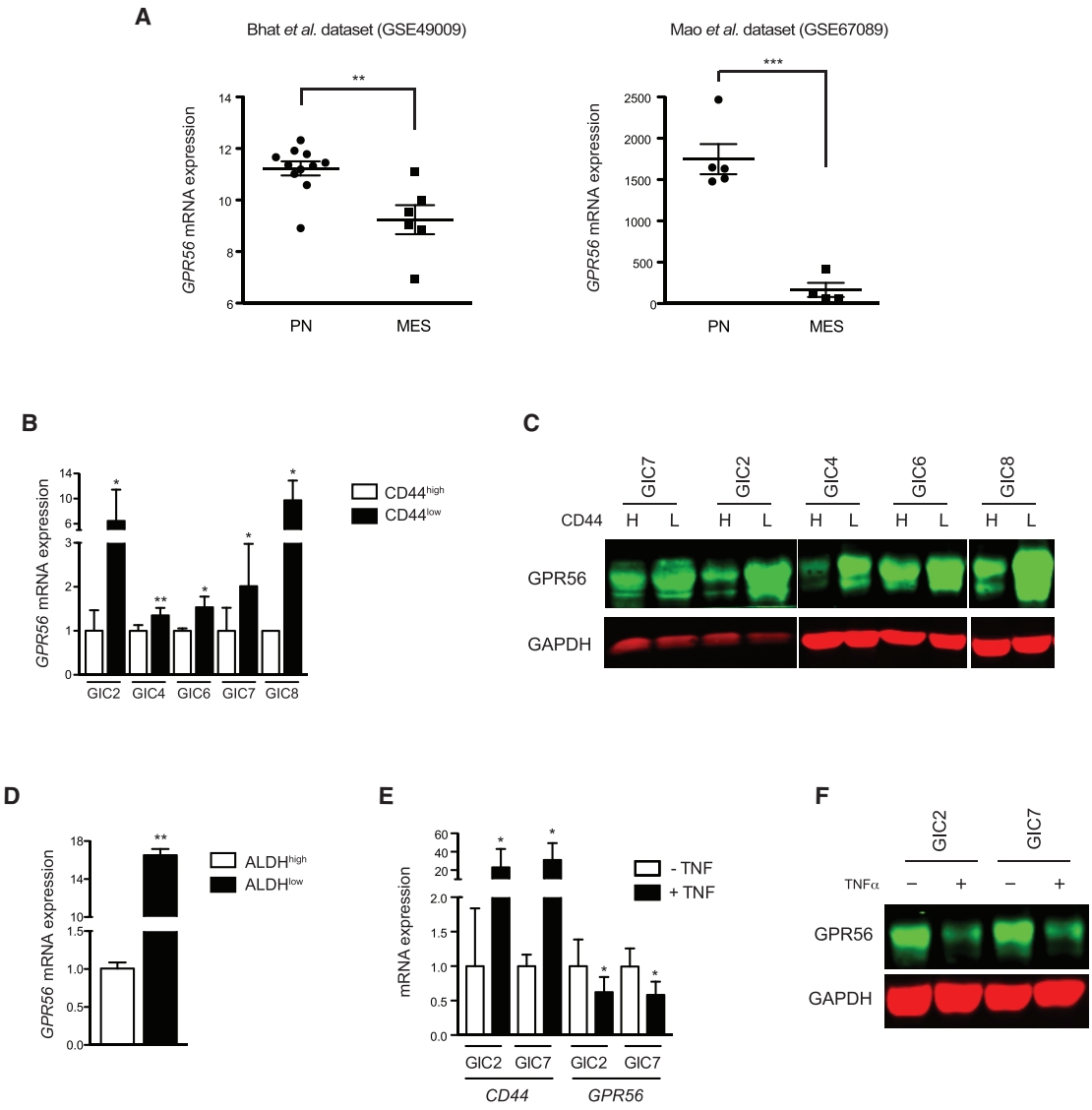

Figure 2. GPR56 Is Highly Expressed in PN-GICs and Downregulated during Their MES Transition in Response to TNF-α

(A) *GPR56* mRNA expression analysis in PN-GICs compared to MES-GICs from the following two independent published datasets: GEO: GSE49009 (Bhat et al., 2013) (unpaired t test, **p = 0.0026) and GSE67089 (Mao et al., 2013) (unpaired t test, ***p = 0.0002). Scatter plots represent mean ± SEM.

(B) *GPR56* mRNA expression was measured by RT-qPCR in different GIC lines sorted into $CD44^{high}$ and $CD44^{low}$ subpopulations. Data are represented as means ± SEMs of at least three independent experiments (t test, *p < 0.05, **p < 0.01).

(C) Western blot analysis of GPR56 in different GIC lines sorted into $CD44^{high}$ and $CD44^{low}$ subpopulations. GAPDH was used as loading control.

(D) *GPR56* mRNA expression was measured by RT-qPCR in GICs sorted into $ALDH^{high}$ or $ALDH^{low}$ populations. Data are represented as means ± SEMs of three independent experiments (t test, **p < 0.005).

(E) *GPR56* and *CD44* mRNA expression was measured by RT-qPCR in $CD44^{low}$ GIC2 and GIC7 treated with or without TNF-α (10 ng/mL for 96 hr). Data are represented as means ± SEMs of at least three independent experiments (t test, *p < 0.05).

(F) Western blot analysis of GPR56 in $CD44^{low}$ GICs treated with or without TNF-α (10 ng/mL for 24 hr). GAPDH was used as a loading control.

See also Figure S2.

of GPR56 in $CD44^{low}$ PN-GICs (Figures S3A and S3B). In line with our previous results, knockdown of GPR56 in $CD44^{low}$ cells led to an increase in CD44 expression both at the mRNA and protein levels (Figures 3A and 3B). Interestingly, the TNF-α-mediated increase in CD44 expression was enhanced by GPR56 knockdown (Figures 3A and 3B), thereby suggesting that GPR56 inhibits the expression of the MES marker CD44. To rule out off-target effects of the GPR56 shRNA, we obtained GPR56-knockout-GIC lines by CRISPR/Cas9 gene editing in $CD44^{low}$ PN-GICs (Figure S3C). In agreement with the GPR56 knockdown experiments, knockout of GPR56 also promoted an increase in CD44 expression both at the mRNA and protein

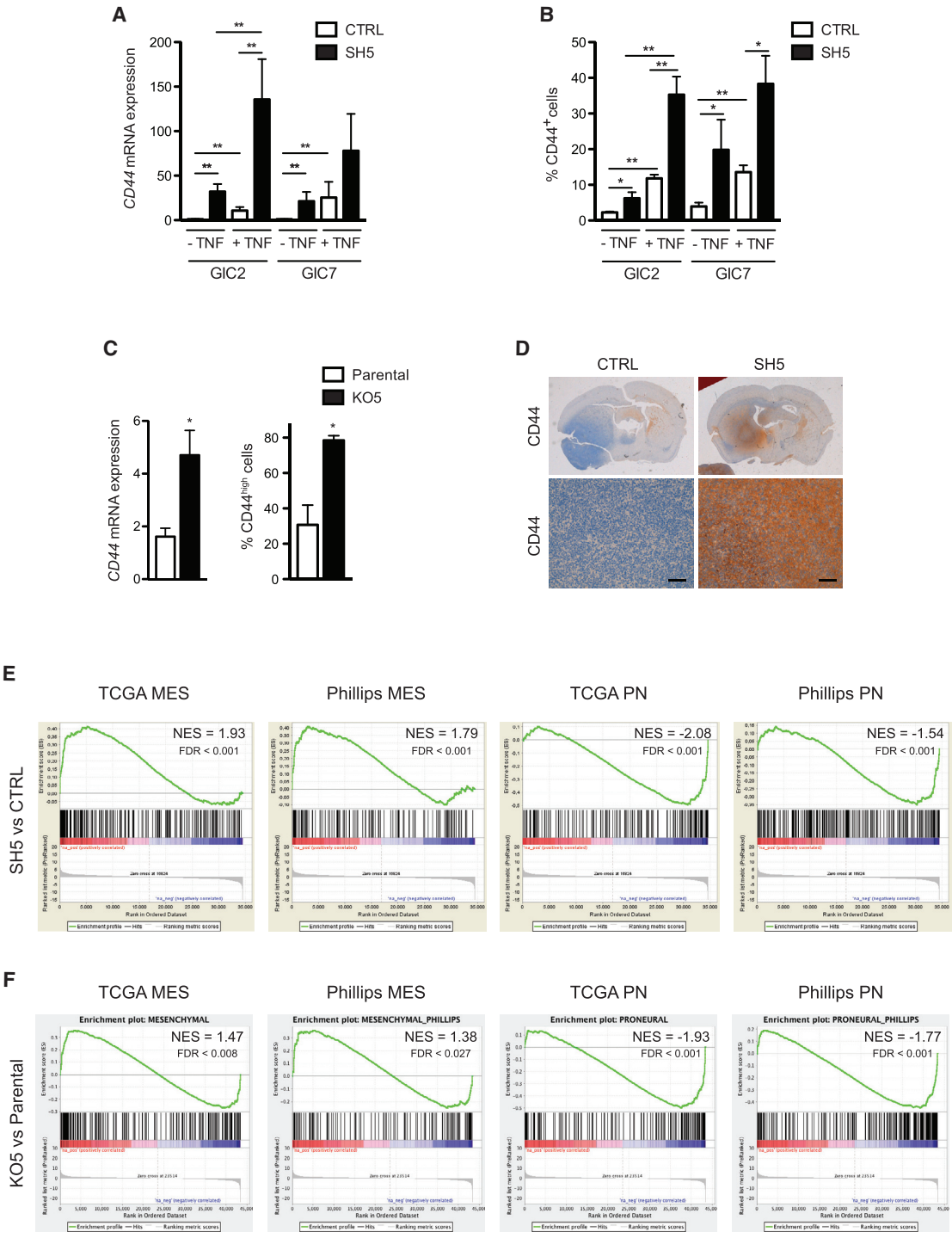

Figure 3. Loss of GPR56 Promotes CD44 Enrichment and MES Differentiation *In Vitro* and *In Vivo*

(A) *CD44* mRNA expression was measured by RT-qPCR in CD44^{low} control (CTRL) or GPR56 knockdown (SH5) GICs treated with or without TNF-α for 4 days. Data are represented as means ± SEMs of at least three independent experiments (t test, **p < 0.01).

(B) Fluorescence activated cell sorting (FACS) analysis of CD44-positive cells in CD44^{low} GPR56 knockdown or control GICs treated with or without TNF-α for 4 days. Data are represented as means ± SEMs of at least three independent experiments (t test, *p < 0.05, **p < 0.01).

(C) Left: *CD44* mRNA expression was measured by RT-qPCR in GPR56 knockout or parental GIC7 (knockout clone KO5 is shown). Right: FACS analysis of the percentage of CD44^{high} cells in GPR56 knockout or parental GIC7. Data are represented as means ± SEMs of three independent experiments (t test, *p < 0.05).

(legend continued on next page)

levels (Figures 3C, S3C, and S3D). To investigate the effect of GPR56 knockdown on CD44 levels *in vivo*, we injected GPR56 knockdown or control GICs into the cerebrum of immunocompromised mice. Orthotopic tumors formed by intracranial injection of GPR56 knockdown-GICs expressed higher levels of CD44 than did control GIC-induced tumors (Figure 3D).

To further test whether GPR56 suppresses MES differentiation, we examined the expression of melanoma cell adhesion molecule (MCAM), which is another MES marker, in response to GPR56 knockdown. Concordantly, GPR56 knockdown GICs expressed higher levels of MCAM protein than did control GICs (Figure S3E), similar to what was observed with CD44. Likewise, the effect of GPR56 knockdown on MCAM expression was enhanced by the presence of TNF-α (Figure S3E). Taken together, our results show that GPR56 knockdown in PN-GICs promotes the expression of the MES markers CD44 and MCAM.

To examine the general role of GPR56 as an inhibitor of MES differentiation, we next induced GPR56 knockdown in a CL-GIC cell line. As in PN-GICs, GPR56 knockdown in CL-GICs promoted an increase in CD44 expression both at the mRNA and protein levels (Figure S3F).

To further characterize the global MES transcriptional program induced by GPR56 knockdown, we performed a whole-genome microarray analysis of gene expression of paired GPR56 knockdown GICs and control GICs. A paired, two-class significance analysis of microarrays (SAMs) (Tusher et al., 2001) identified 117 genes that were differentially expressed between knockdown and control cells (53 upregulated and 64 downregulated) (Table S2). As expected, *GPR56* was significantly downregulated in the knockdown samples. In a gene set enrichment analysis (GSEA) (Subramanian et al., 2005) using two previously published PN and MES signatures (Phillips et al., 2006; Verhaak et al., 2010), we observed that GPR56 knockdown GICs were positively enriched for genes in the MES gene sets and, conversely, negatively enriched in PN genes (Figure 3E). This same pattern emerged in a GSEA using KO5-GIC microarray datasets wherein a positive association with MES genes and a negative association with PN genes were observed in GPR56 knockout GICs (Figure 3F). These results further support the notion that GPR56 is an inhibitor of MES differentiation in GICs.

We confirmed the global alteration in gene expression that was shown via a GSEA of microarray data using an RT-qPCR analysis of a previously reported MES gene set (Bhat et al., 2013). Most MES genes were upregulated upon GPR56 knockdown in $CD44^{low}$ GICs (Figure S4A). Interestingly, the GPR56 knockdown-induced increase in MES gene expression was larger than that induced by TNF-α treatment alone (Figure S4B). The induction of the MES signature upon GPR56 knockdown was also observed in unsorted GICs although to a much lesser extent, thus suggesting that GPR56 loss mainly affects the $CD44^{low}$ population (Figure S5A). Moreover, the increase in MES gene expression was enhanced in GPR56 knockdown cells in the presence of TNF-α (Figure S5B). In agreement with the GPR56 knockdown data, we observed that most MES markers were also upregulated in GPR56 knockout GICs (Figure S5C). Furthermore, GPR56 knockdown in CL-GICs also induced an increase in gene expression of several MES markers (Figure S5D). Taken together, our results suggest that GPR56 may be a general inhibitor of MES differentiation in non-MES GICs including PN- and CL-GICs.

Knockdown of GPR56 Promotes Radioresistance *In Vitro* and *In Vivo*

We next interrogated whether GPR56 also regulates properties that are associated with a MES phenotype. MES differentiation has been linked to resistance to therapy. Several EMT inducers, such as NF-κB or ZEB1, are associated with increased radioresistance or chemoresistance (Bhat et al., 2013; Siebzehnrubl et al., 2013). Therefore, we asked whether GPR56 is involved in the acquisition of radioresistance.

Because ionizing radiation (IR) has been shown to induce PMT (Halliday et al., 2014; Mao et al., 2013), we first examined whether IR enhances MES differentiation in our PN-GIC cultures by measuring the expression of the MES marker MCAM. As expected, control-GICs upregulated MCAM expression in response to IR. Interestingly, the IR-induced increase in MCAM expression was enhanced in GPR56 knockdown GICs (Figure 4A), analogously to the increased MES differentiation upon GPR56 knockdown in TNF-α-treated GICs (Figure S3E).

Next, we examined whether knockdown of GPR56 was sufficient to lead to radioresistance. In response to IR, PN-GICs usually undergo a profound arrest in G2/M (Bhat et al., 2013; Mir et al., 2010). On the contrary, MES-GICs only display a modest arrest in G2/M upon exposure to IR, which was correlated with a faster ability to repair DNA damage as measured by γ-H2AX foci formation (Bhat et al., 2013). Concordant to the acquisition of a MES phenotype in GPR56 knockdown GICs, the percentage of cells in G2/M after IR was significantly lower in GPR56 knockdown GICs than in control GICs (Figure 4B). We then measured the kinetics of γ-H2AX foci formation and repair in GPR56 knockdown GICs versus control GICs. Although both cell lines showed comparable γ-H2AX foci formation at early time-points, GPR56 knockdown GICs showed an enhanced repair ability 24 and 48 hr after IR exposure (Figure 4C).

Finally, to test whether GPR56 knockdown GICs have increased radioresistance *in vivo*, we examined the effect of clinically relevant fractionated doses of IR (2.5 Gy × 4) on orthotopic tumors induced by intracranial injection of control or GPR56 knockdown GICs in immunocompromised mice.

(D) Immunohistochemistry of CD44 in orthotopic tumors induced by intracranial injection of control or GPR56 knockdown GICs into the brain of immunocompromised nude mice. Representative stainings of four injected mice per group are shown. Scale bar, 100 μm.
(E) GSEA enrichment plots of MES and PN signatures (TCGA-Verhaak and Phillips) in GPR56 knockdown versus control GICs. Normalized enrichment score (NES) and FDR are shown for each plot.
(F) GSEA enrichment plots of MES and PN signatures (TCGA-Verhaak and Phillips) in GPR56 knockout versus parental GICs. NES and FDR are shown for each plot.
See also Figures S3–S5 and Table S2.

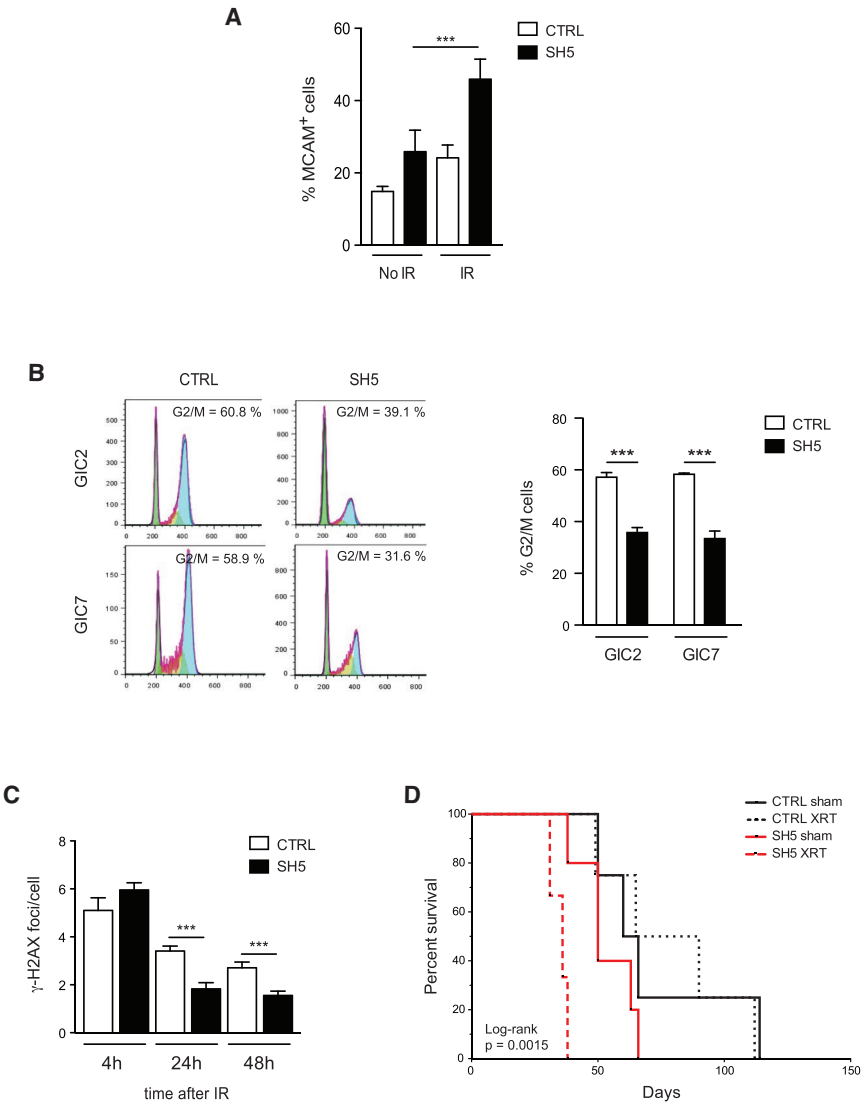

Figure 4. Knockdown of GPR56 Promotes Radioresistance

(A) FACS analysis of MCAM-positive cells in GPR56 knockdown GICs or control GICs after exposure to 6 Gy ionizing radiation (IR). Data are represented as means ± SEMs of at least three independent experiments (t test, ***$p < 0.001$).

(B) Cell cycle analysis of GPR56 knockdown- and control-GICs. Left: cell cycle plots. The percentage of cells in G2/M phase is indicated within each plot. Right: percentages of cells in G2/M in GPR56 knockdown or control GICs. Data are represented as means ± SEMs of at least three independent experiments (ANOVA, ***$p < 0.0001$).

(C) γ-H2AX foci formation assay of GPR56 knockdown or control GICs 24 or 48 hr after exposure to 3 Gy IR. Data are represented as means ± SEMs of 15–16 technical replicates of two independent experiments (t test, ***$p < 0.001$).

(D) Kaplan-Meier survival curves of mice implanted with GPR56 knockdown or control GIC2 and treated with or without fractioned intracranial radiation (2.5 Gy × 4). A log-rank test was used to assess statistical significance ($p = 0.0015$).

Control-GIC-injected animals had higher survival rates than did GPR56-knockdown-tumor-bearing mice. The former showed a slightly improved median survival upon IR treatment, although it was not statistically significant (Figure 4D). Interestingly, IR treatment exacerbated the poor survival rates of GPR56-knockdown-GIC-injected mice, thereby suggesting that GPR56 knockdown GICs are highly radioresistant (Figure 4D). Taken together, these results suggest that GPR56 silencing promotes he radioresistance of PN-GICs both *in vitro* and *in vivo*.

GPR56 Prevents MES Differentiation by Inhibiting NF-κB Signaling

The NF-κB signaling pathway is one of the main regulators of the MES differentiation in response to TNF-α (Bhat et al., 2013; Edwards et al., 2011). Since we observed that the TNF-α-induced MES differentiation is enhanced by GPR56 knockdown, we interrogated whether GPR56 interferes with NF-κB signaling. In transcriptional assays using a luciferase reporter controlled by NF-κB binding sites, GPR56 knockdown GICs displayed higher NF-κB activity than did control cells, thereby suggesting that GPR56 inhibits NF-κB-dependent transcriptional activity (Figure 5A).

To further understand the mechanisms by which GPR56 inhibits NF-κB activity, we analyzed the levels of nuclear factor kappa B inhibitor, alpha (IκBα), a canonical inhibitor of the NF-κB signaling pathway (Gilmore, 2006). Interestingly, GPR56 knockdown GICs expressed lower levels of IκBα than did control GICs (Figure 5B). In addition, while TNF-α decreased IκBα levels in control-GICs as expected, the TNF-α-induced reduction of IκBα was enhanced in GPR56 knockdown GICs. These results are in agreement with the synergistic effects of TNF-α and GPR56 knockdown that have been observed on the MES phenotype. We next tested the effect of a constitutively active form of IκBα in the context of GPR56 knockdown (Figure S6A). IκBα super repressor (IκB-SR) is a mutant that cannot be degraded by phosphorylation in response to NF-κB agonists. The induction of CD44 by TNF-α was significantly inhibited by IκB-SR both in control GICs and GPR56 knockdown GICs. Furthermore, GPR56 shRNA was not able to increase CD44 expression in the presence of IκB-SR, indicating that GPR56 inhibits NF-κB signaling upstream of IκBα (Figures 5C and S6B). Therefore, these results suggest that GPR56 might inhibit NF-κB signaling by increasing the levels of IκBα protein.

IκBα protein levels are regulated by the IKK complex, which phosphorylates IκBα and targets it for proteasomal degradation. IKKγ/NF-κB essential modulator (NEMO) is the regulatory

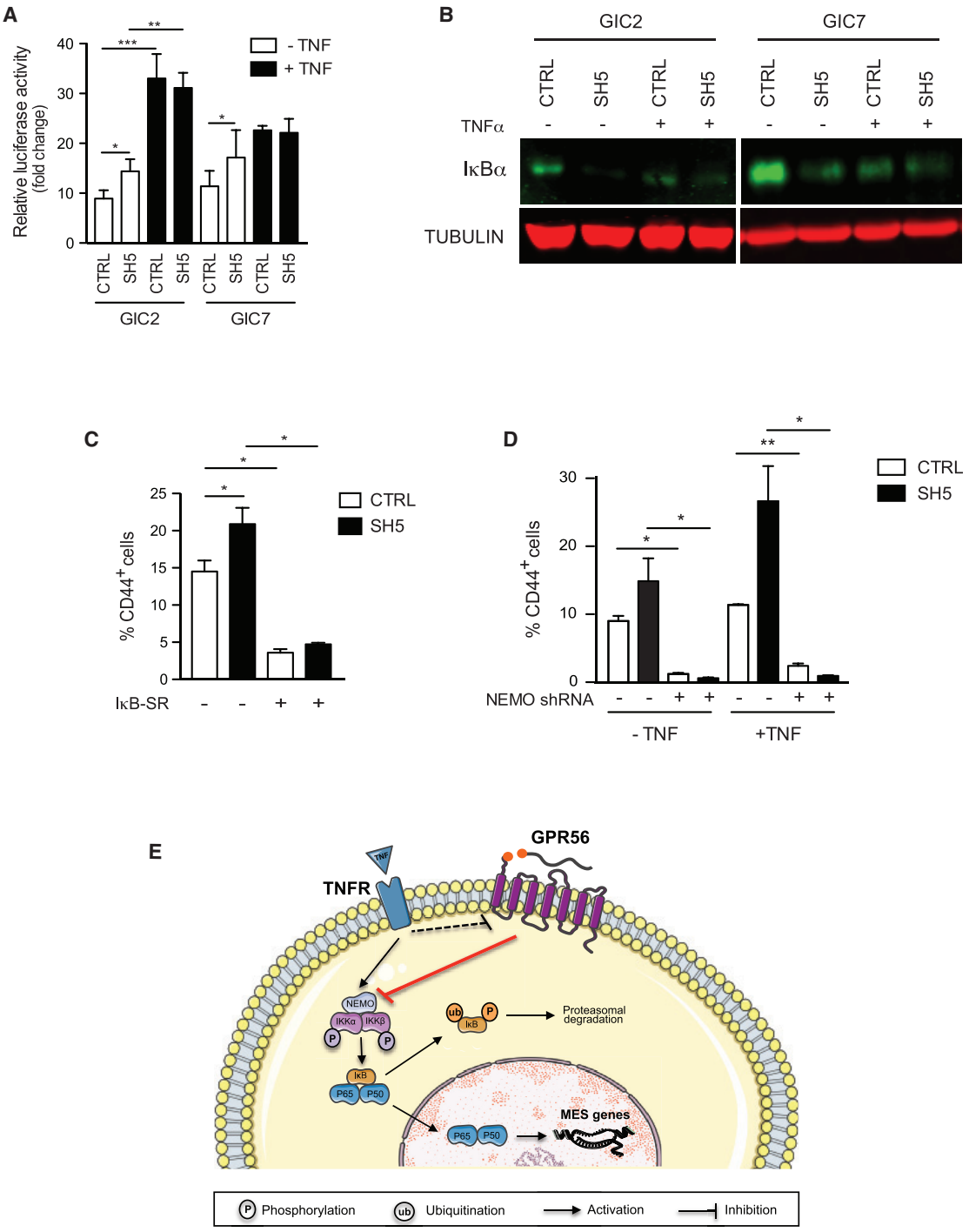

Figure 5. GPR56 Prevents MES Differentiation by Inhibiting NF-κB Signaling

(A) Luciferase activity assay of GPR56 knockdown or control GICs treated with or without TNF-α. Data are represented as means ± SEMs of at least three independent experiments (t test, *p < 0.05, **p < 0.01, ***p < 0.005).

(B) Western blot analysis of IκBα protein levels in CD44^{low} GPR56 knockdown or control GICs treated with or without TNF-α. Tubulin was used as loading control.

(C) FACS analysis of CD44-positive cells in control or GPR56 knockdown GICs (GIC2) infected with control or IκB-SR adenoviruses. Adenoviral infection was performed 24 hr prior to TNF-α treatment for an additional 72 hr. Data are represented as means ± SEMs of at least three independent experiments (t test, *p < 0.05).

(D) FACS analysis of CD44-positive cells in control or GPR56 knockdown GICs stably transduced with NEMO shRNA-encoding lentiviruses and treated with or without TNF-α. Data are represented as means ± SEMs of at least three independent experiments (t test, *p < 0.05, **p < 0.01).

(legend continued on next page)

subunit of the IKK complex. To interrogate whether GPR56 stabilizes IκBα protein by inhibiting the IKK complex, we tested the effect of GPR56 loss in NEMO knockdown GICs (Figure S6C). TNF-α did not induce CD44 expression in NEMO knockdown GICs, as expected for an upstream activator of the NF-κB signaling pathway. In addition, GPR56/NEMO knockdown GICs had similar levels of CD44 as those of control cells both in the absence or presence of TNF-α, indicating that GPR56 inhibits NF-κB signaling upstream of NEMO (Figure 5D).

In summary, our results suggest that GPR56 inhibits NF-κB signaling by inhibiting the IKK complex and, thereby, stabilizing IκBα protein levels. We propose a model in which GPR56 inhibits NF-κB signaling in PN-GICs in the basal state. During MES differentiation, TNF-α directly activates the NF-κB pathway (direct pathway) while also promoting a decrease in GPR56 expression. The latter effect releases the GPR56-mediated IKK inhibition, thereby enhancing NF-κB pathway activation (indirect pathway) (Figure 5E).

Low GPR56 Is a Poor Prognostic Factor in Non-G-CIMP GBM Patients

To test whether our results in experimental cellular and mouse models might be translated to human GBMs, we analyzed whether a GPR56-associated signature correlates with overall survival (OS) or disease-free survival (DFS) in GBM patients of the TCGA dataset. A gene-expression-based signature associated with a low expression of GPR56 was derived using the 117 differentially expressed genes in control versus GPR56 knockdown GICs. This signature was applied onto the TCGA gene expression dataset (Brennan et al., 2013) by calculating a low GPR56-associated signature score for each GBM patient in the dataset (see Experimental Procedures). Interestingly, GBM patients (G-CIMP and non-G-CIMP) with a low GPR56-associated signature displayed shorter OS and DFS than did patients whose tumors had a high GPR56-associated signature (Figure 6A). To exclude the possibility that G-CIMP tumors that were included in the analysis were responsible for the improved survival phenotype, we also analyzed this signature only within non-G-CIMP GBMs. Importantly, the low GPR56-associated signature was also correlated with poor survival in non-G-CIMP GBMs (Figure 6B). Median OS was shorter in non-G-CIMP tumors with a low GPR56-associated signature versus GBMs with a high GPR56-associated signature. Median DFS was also shorter in non-G-CIMP GBMs with a low GPR56-associated signature.

To validate these results in an independent dataset, we analyzed the correlation of GPR56 levels (as measured by immunohistochemistry) with survival in GBM patients from the Ohio State University dataset (Mao et al., 2013). In line with the results obtained with the TCGA dataset, GBM patients with high levels of GPR56 displayed increased OS compared with that of those with low or intermediate levels of GPR56 protein (Figure 6C). Taken together, our results suggest that GBM patients with low GPR56 expression have a worse prognosis, which might be explained by the increased radioresistance of GPR56^{low}-GICs in these tumors.

According to the low expression of *GPR56* in MES-GBMs (Figure 1A), these tumors displayed a high score for the low GPR56-associated signature compared with the rest of GBM subtypes (Figure 6D). These results further support the notion that MES-GBMs have worse prognosis than do non-MES-GBMs.

A Low GPR56-Associated Signature Is Associated with MES Signatures across Multiple Tumor Types beyond GBM

To interrogate whether GPR56 might also inhibit MES differentiation in other tumor types, we analyzed the expression of the low GPR56-associated signature across 25 different tumor types (TCGA datasets) and correlated this signature with 414 previously published oncogenic signatures (Prat et al., 2015). Strikingly, we found a significant correlation between the low GPR56-associated signature and signatures related to MES phenotypes, such as CD44^{+} breast cancer stem cells (Creighton et al., 2009) or EMT (Taube et al., 2010), in the great majority of tumors (Figures 7A and 7B). Conversely, the low GPR56-associated signature was negatively correlated with signatures related to epithelial differentiation (Prat et al., 2010) and proliferation (Fan et al., 2011; Prater et al., 2014; Wirapati et al., 2008) (Figures 7A and 7B). Interestingly, there was a positive correlation between the low GPR56-associated signature and inflammatory signatures (Iglesia et al., 2016; Iglesia et al., 2014; Rody et al., 2009; Van Laere et al., 2013), which correlates with the increased inflammatory infiltrates in MES-like tumors. From these results, we infer that GPR56 might have a general role as an inhibitor of the MES transition across multiple tumor types beyond GBM, presumably through the inhibition of NF-κB signaling.

Furthermore, we also performed a pan-cancer survival analysis of tumors with a low GPR56-associated signature (12 tumor types; TCGA datasets). Impressively, the low GPR56-associated signature had a prognostic value in the following four tumor types: breast cancer (BRCA), GBM, lung squamous cell carcinoma (LUSC), and uterine corpus endometrioid carcinoma (UCEC). As in GBM patients, LUSC patients whose tumors expressed high levels of the low GPR56-associated signature had a poor prognosis. Conversely, a low GPR56-associated signature was predictive of better outcomes in BRCA and UCEC. These results suggest that GPR56 might have a major role in the biology of cancer cells in a broad range of tumor types.

DISCUSSION

GBMs are highly plastic and have an inherent tendency to transition from one subtype to another (Bhat et al., 2013; Kupp et al., 2016; Lu et al., 2016; Mao et al., 2013). This transcriptional

(E) Proposed molecular interactions between GPR56 and NF-κB signaling. In the basal state, GPR56 inhibits the NF-κB signaling pathway upstream of NEMO. TNF-α activates NF-κB signaling, thereby promoting the transcriptional activation of mesenchymal genes (direct pathway). At the same time, TNF-α promotes GPR56 downregulation, thereby relieving GPR56-mediated NF-κB inhibition and enhancing MES differentiation (indirect pathway).
See also Figure S6.

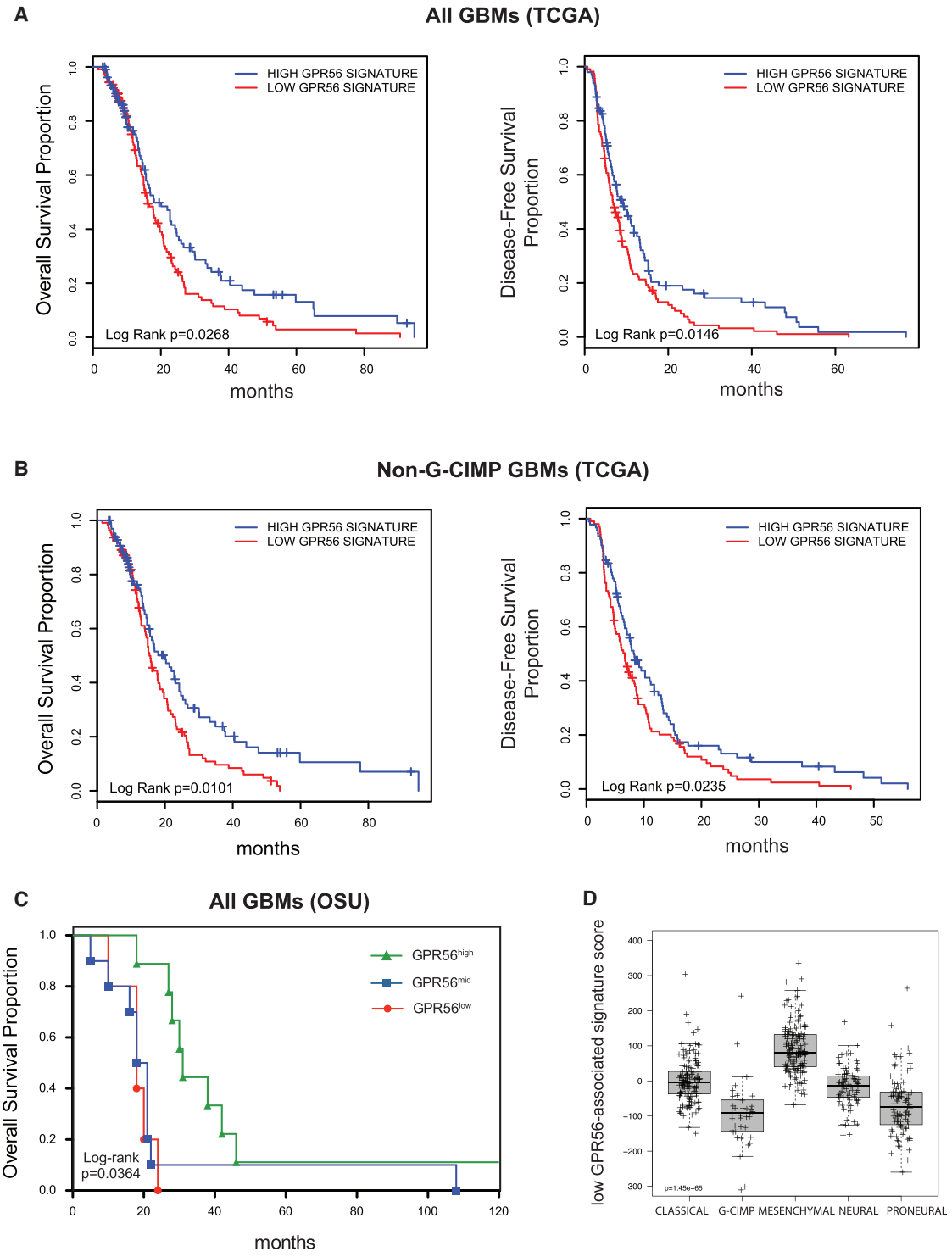

Figure 6. Low GPR56-Associated Signature Correlates with Poor Survival in Human GBM

(A) Kaplan-Meier curves showing (left) overall survival (OS) and (right) disease-free survival (DFS) of GBMs (G-CIMP and non-G-CIMP) enriched in the low GPR56-associated signature (low GPR56 signature) versus GBMs with low expression of this signature (high GPR56 signature) (TCGA dataset).

(B) Kaplan-Meier curves showing OS (left) and DFS (right) of non-G-CIMP GBMs enriched in the low GPR56-associated signature versus GBMs with low expression of this signature (TCGA dataset).

(A and B) Patients were divided into two groups (high or low GPR56 signature) according to their low GPR56-associated signature score (cutoff: median of the signature score).

(legend continued on next page)

plasticity empowers GBMs with the capability to adapt to treatment and develop resistance to therapy and holds the key to understand the extreme resilience of GBMs to any oncologic treatment. The identification of the molecular mechanisms that control transitions from one subtype to another is crucial to understand GBM natural evolution and acquired resistance to therapy. In this study, we identified GPR56/ADGRG1 as an inhibitor of the MES transition in GICs. GPR56 is an adhesion GPCR with a prominent role in NSC and OPC proliferation and differentiation (Ackerman et al., 2015; Bae et al., 2014; Giera et al., 2015) and is highly expressed in PN and CL GBMs (Figure 1A). These findings are in agreement with the proposed role of NSCs or OPCs as the cells of origin of PN-GBMs (Alcantara Llaguno et al., 2015; Liu et al., 2011) and with an NSC-like behavior of CL-GICs (Kupp et al., 2016). Our study highlights the central role in GBM pathogenesis of factors that control normal neural progenitor functions.

MES differentiation in GBMs is associated with increased radioresistance (Bhat et al., 2013), and accordingly, we also showed that GPR56 inhibits radioresistance. In addition, we identified a low GPR56-associated signature that is prognostic of a poor outcome in non-G-CIMP GBM patients who were treated with radiotherapy. Therefore, our studies might represent a starting point in designing gene-expression-based diagnostic tools to predict the GBM response to radiotherapy. Hyperactivation of NF-κB signaling has been associated with MES-subtype GBMs (Bhat et al., 2013; Verhaak et al., 2010). Therefore, the NF-κB pathway is regarded as a promising target for drug development in many cancer types including MES-GBMs (Prasad et al., 2010). Mechanistically, we uncovered that GPR56 inhibits canonical NF-κB signaling by inhibiting the IKK complex and, thus, stabilizing IκBα protein levels. Given the GPR56/NF-κB signaling link, and since GPR56 is a member of the Adhesion-GPCR class, our study robustly provides a druggable therapeutic target in the development of adjuvant therapies to overcome radioresistance in GBM and possibly other cancers. Furthermore, the identification of the GPR56/NF-κB signaling axis may have important consequences in other fields beyond cancer biology where NF-κB and GPR56 have major regulatory roles, such as innate and adaptive immunity or neural progenitor biology (Ackerman et al., 2015; Bae et al., 2014; Chang et al., 2016; Giera et al., 2015; Piao et al., 2004).

The classification of tumors into subtypes with clinical meaning is of crucial interest for clinical diagnostics as well as to predict responses to treatments and eventually develop patient-tailored therapies. The TCGA project identified five distinct molecular subtypes in GBM according to their gene expression and epigenetic profiles (Brennan et al., 2013; Noushmehr et al., 2010; Verhaak et al., 2010). The epigenetic G-CIMP phenotype is predictive of longer survival (Noushmehr et al., 2010). Conversely, MES-related gene signatures have been associated with higher GBM aggressiveness although most studies have included G-CIMP tumors (Cheng et al., 2012; Gerber et al., 2014; Kim et al., 2013), which are associated with a PN (non-MES) phenotype and might have been a confounding factor in these studies. In a step further, we previously showed a significant correlation between a MES composite metagene and shorter survival or radioresistance in patients with *IDH* wild-type GBMs, which largely overlap with the non-G-CIMP group (Bhat et al., 2013). Recently, Wang et al. (2017) have refined the GBM-intrinsic transcriptional subtype classification and confirmed that, among primary and recurrent *IDH* wild-type GBMs, the MES subtypes had the worst prognosis. Importantly, in this study, we found that a low GPR56-associated signature is associated with a poor patient prognosis within non-G-CIMP GBMs. Because GPR56 is an important player in MES differentiation, our results strengthen the idea that gene signatures that are associated with MES features may be clinically used to predict GBM patient survival and highlight the great importance of understanding the molecular mechanisms that regulate MES differentiation. Noticeably, we showed that a functional signature (low GPR56 signature) that is linked to a biologically relevant signaling pathway has a robust prognostic value. These results highlight the fact that understanding the biology behind the different GBM subtypes is crucial to predict tumor behavior at the clinical level.

In a pan-cancer analysis, we showed that the low GPR56-associated signature was positively correlated with MES signatures, and it even had a prognostic value in other tumor types beyond GBM (Figure 7). Strikingly, GPR56 is downregulated in claudin-low breast tumors, which are associated with poorer prognosis and display features of MES and inflammatory phenotypes (Prat et al., 2010). Our results suggest that GPR56 might have a general regulatory role in cancer cell biology, presumably through the maintenance of the epithelial state and the inhibition of a MES fate. Further studies addressing the function of GPR56 in other tumor types are required to test this hypothesis.

EXPERIMENTAL PROCEDURES

Cell Culture and Treatments

Cell cultures that were enriched in GICs were obtained from human GBM specimens as described previously (Alonso et al., 2011; Galli et al., 2004) and subsequently cultured on laminin-coated plates (10 μg/mL; Sigma) and maintained in Dulbecco's Modified Eagle Medium: Nutrient Mixture F-12 (DMEM/F12; GIBCO) supplemented with N2 (GIBCO), basic fibroblast growth factor, and epidermal growth factor (20 ng/ml; GIBCO) at 37°C, 5% CO_2, and 5% oxygen. Lentiviral or retroviral transduction was performed by treating cells with the purified viral suspension for 4 hr. Cells were selected with the appropriate drug 48 hr post-infection. For cytokine treatment, GICs were

(C) Kaplan-Meier curves showing OS of GBMs displaying either high (n = 9), intermediate (n = 10), or low (n = 5) levels of GPR56 as assessed by immunohistochemistry (Ohio State University dataset).

(D) Expression of the low GPR56-associated signature across the different subtypes of GBM was calculated using gene expression data from the TCGA dataset (Brennan et al., 2013). Shown is a boxplot diagram of the low GPR56-associated signature score for each GBM patient in the dataset (Table S2). Differences in the low GPR56-associated signature score among subtypes were assessed with the Kruskal-Wallis rank sum test (Dunn's post hoc multiple-comparison test: MES versus each of the other subtypes, $p < 0.0001$). In the box-plots, the horizontal line indicates the median, boundaries of the box indicate the first and third quartiles, and whiskers indicate confidence intervals (95%).

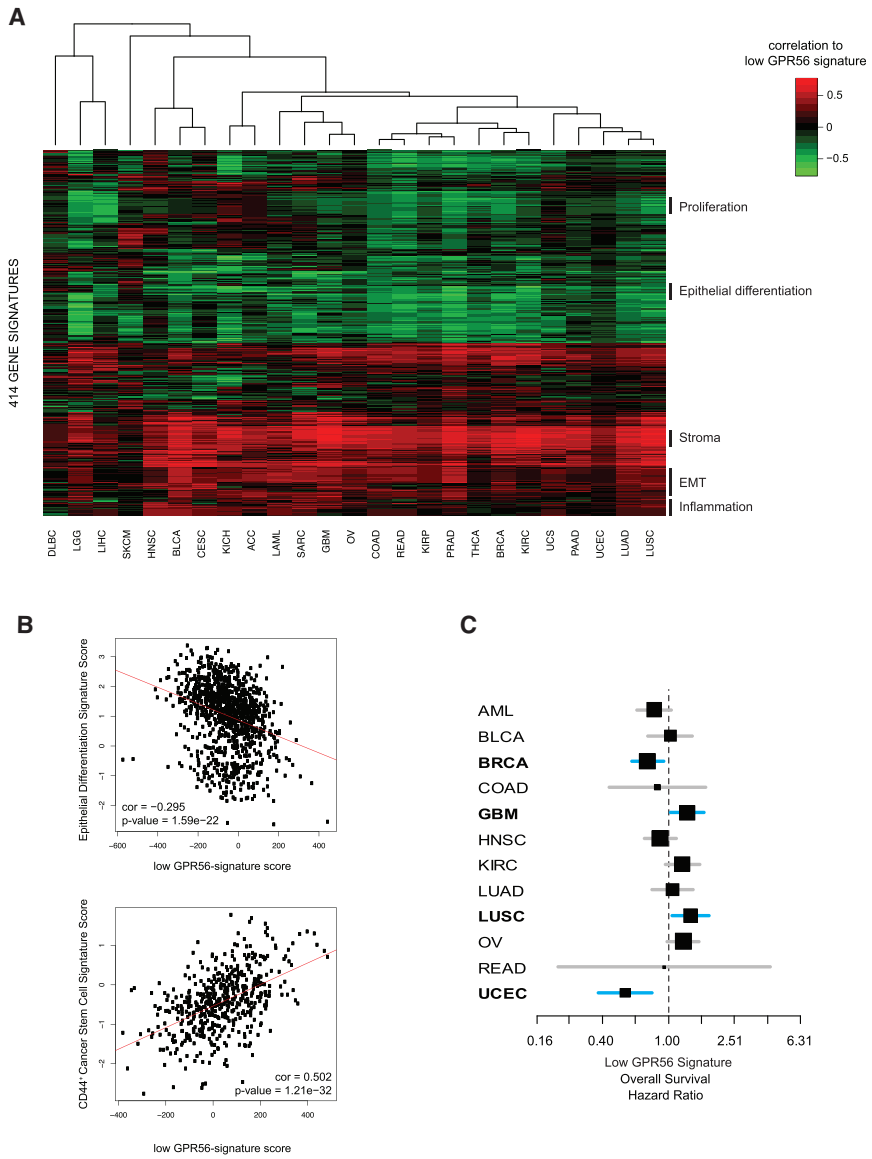

Figure 7. A Low GPR56-Associated Signature Correlates with MES Signatures across Different Tumor Types

(A) Correlations between the low GPR56-associated signature and each of 414 gene signatures from the University of North Carolina (UNC) database (Table S3; Prat et al., 2015) across 25 different tumor types (TCGA datasets). Shown is a clustered heatmap of Pearson's correlation coefficient values. Acronyms of tumor types are described in Table S3.

(B) Representative individual correlation plots between the low GPR56-associated signature and selected gene signatures (epithelial differentiation (UNC_Differentiation.Score_Model_BCR.2010) or $CD44^+$ breast cancer stem cells (UNC_MS_CD44_UP_Median_PNAS.2009) in either breast cancer (BRCA) or lung squamous cell carcinoma (LUSC), respectively. Pearson's correlation coefficients and p values are shown within each plot.

(C) Pan-cancer survival analysis of tumors with a low GPR56-associated signature. The plot shows the overall survival hazard ratios of patients whose tumors express high levels of the low GPR56-associated signature. The size of the square is inversely proportional to the SE. Horizontal bars represent 95% CIs of hazard ratios. In blue, the associations were found to be statistically significant.

See also Table S3.

treated with 10 ng/mL of TNF-α (Peprotech) for different time periods as indicated in figure legends.

Orthotopic Xenograft Models

A total of 1×10^5 GICs constitutively expressing luciferase were injected intracranially into the right striatum of 4–6 week-old male athymic nude mice anesthetized with ketamine and xylacine. Stereotaxic coordinates used were 0.5 mm lateral, 2 mm anterior from the bregma, and 3 mm deep. Intracranial tumor growth was monitored by non-invasive bioluminescence imaging using the Aequoria MDS system (Hamamatsu). When appropriate, mice were sacrificed, and brain sections were stained with H&E and subjected to immunohistochemistry. All animal procedures were reviewed and approved by the Institutional Animal Care and Use Committee at the University of Barcelona.

For the *in vivo* irradiation experiments, GICs were implanted intracranially using the guide-screw system in 4–5 week-old athymic nude mice (male/female randomized). After 1 week of guide-screw implantation, 5×110^5 cells were injected intracranially in each mouse and randomly distributed between groups. A minimum of five mice was used in each group. Kinetics of tumor growth were monitored using IVIS 200 system bioluminescent imaging, and tumor volume was measured using Living Image 4.1 software. IR was delivered using fractionated doses (2.5 Gy × 4) using a ^{60}Co teletherapy unit and a custom gig with validated dosimetry. Mice that presented neurological symptoms (i.e., hydrocephalus, seizures, inactivity, or ataxia) or that were moribund were sacrificed, and brains were fixed in formalin and stained with H&E to confirm the presence of a tumor. All animal procedures were reviewed and approved by the Institutional Animal Care and Use Committee at the M.D. Anderson Cancer Center.

Bioinformatic Analysis of Microarray Data

To identify genes that were differentially expressed across groups, normalized microarray data were analyzed using a multiclass SAM (Tusher et al., 2001). The low GPR56-associated signature was defined as the 117 genes that were differentially expressed between GPR56 knockdown and control cells (53 upregulated and 64 downregulated; Table S2). To obtain an enrichment score that was related to the low GPR56-associated signature for each sample or patient, the SAM score of each gene in the signature was multiplied by its expression value in the tested sample, and all these values were summed up to give a single score as described in Gómez-Miragaya et al. (2017) and Keller et al. (2012).

Statistical Analysis

Two-tailed Student's t test (to compare two experimental groups) or an ANOVA (to compare three or more groups) were performed for data analysis using GraphPad Prism (GraphPad Software). A Kruskal-Wallis test was used for gene expression data analysis from GBM patients (TCGA dataset), whereas a log-rank analysis was performed to determine the statistical significance of Kaplan-Meier survival curves using the R statistics software (The R Project for Statistical Computing). For all statistical methods, $p < 0.05$ was considered significant.

DATA AND SOFTWARE AVAILABILITY

The accession numbers for the microarray data reported in this paper are GEO: GSE94765 (GPR56 knockdown versus control GICs) and GSE104653 (GPR56 knockout versus parental GICs).

SUPPLEMENTAL INFORMATION

Supplemental Information includes Supplemental Experimental Procedures, six figures, and three tables and can be found with this article online at https://doi.org/10.1016/j.celrep.2017.10.083.

AUTHOR CONTRIBUTIONS

M. Moreno. and N.d.l.I. performed and analyzed experiments and wrote the manuscript. L. Pedrosa, L.B., J.M., V.B., R.E., N.K., S.-H.K., J.W., A.A., S.C., and H.M. performed experiments. L. Paré, E.P., T.P., A.P., and K.P.B. analyzed experiments. M. Marin, A.H., A.T., and F.G. contributed to experiments. T.R., M.M.A., C.G.-M., E.P.S., I.N., and K.P.B. provided clinical specimens and patient-derived cell lines. K.P.B., A.P., X.P., I.N., and H.M. provided expertise and feedback and reviewed the manuscript. N.d.l.I. conceived and supervised the research project.

ACKNOWLEDGMENTS

We thank Dr. Rossella Galli for sharing her GIC lines, Dr. Lluís Espinosa for his advice on NF-κB signaling, and Jordi Solà and César Herreros, from the Radiation Oncology Department at Hospital Clínic of Barcelona, for their help with the cell irradiation experiments. This work was supported by grants from the Spanish Ministry of Economy and Competitiveness (MINECO) (BFU2009-14616 and RyC-09-389-10-01 to N.d.l.I.), Fundación Ramón Areces (CIVP16A1850 to N.d.l.I.), and an FPI predoctoral fellowship from MINECO (to M. Moreno). This research was also supported by NIH grant R01NS083767 (to I.N.) and the University Cancer Foundation via the Institutional Research Grant program and start-up funds at the University of Texas M.D. Anderson Cancer Center (to K.P.B.). This work was co-funded by the European Regional Development Fund (ERDF) and the CERCA Programme (Generalitat de Catalunya).

Received: March 21, 2017
Revised: September 7, 2017
Accepted: October 23, 2017
Published: November 21, 2017

REFERENCES

Ackerman, S.D., Garcia, C., Piao, X., Gutmann, D.H., and Monk, K.R. (2015). The adhesion GPCR Gpr56 regulates oligodendrocyte development via interactions with Gα12/13 and RhoA. Nat. Commun. *6*, 6122.

Alcantara Llaguno, S.R., Wang, Z., Sun, D., Chen, J., Xu, J., Kim, E., Hatanpaa, K.J., Raisanen, J.M., Burns, D.K., Johnson, J.E., and Parada, L.F. (2015). Adult lineage-restricted CNS progenitors specify distinct glioblastoma subtypes. Cancer Cell *28*, 429–440.

Alonso, M.M., Diez-Valle, R., Manterola, L., Rubio, A., Liu, D., Cortes-Santiago, N., Urquiza, L., Jauregi, P., Lopez de Munain, A., Sampron, N., et al. (2011). Genetic and epigenetic modifications of Sox2 contribute to the invasive phenotype of malignant gliomas. PLoS ONE *6*, e26740.

Bae, B.I., Tietjen, I., Atabay, K.D., Evrony, G.D., Johnson, M.B., Asare, E., Wang, P.P., Murayama, A.Y., Im, K., Lisgo, S.N., et al. (2014). Evolutionarily dynamic alternative splicing of GPR56 regulates regional cerebral cortical patterning. Science *343*, 764–768.

Bhat, K.P., Salazar, K.L., Balasubramaniyan, V., Wani, K., Heathcock, L., Hollingsworth, F., James, J.D., Gumin, J., Diefes, K.L., Kim, S.H., et al. (2011). The transcriptional coactivator TAZ regulates mesenchymal differentiation in malignant glioma. Genes Dev. *25*, 2594–2609.

Bhat, K.P.L., Balasubramaniyan, V., Vaillant, B., Ezhilarasan, R., Hummelink, K., Hollingsworth, F., Wani, K., Heathcock, L., James, J.D., Goodman, L.D., et al. (2013). Mesenchymal differentiation mediated by NF-κB promotes radiation resistance in glioblastoma. Cancer Cell *24*, 331–346.

Brennan, C.W., Verhaak, R.G., McKenna, A., Campos, B., Noushmehr, H., Salama, S.R., Zheng, S., Chakravarty, D., Sanborn, J.Z., Berman, S.H., et al. (2013). The somatic genomic landscape of glioblastoma. Cell *155*, 462–477.

Bundy, L.M., and Sealy, L. (2003). CCAAT/enhancer binding protein beta (C/EBPbeta)-2 transforms normal mammary epithelial cells and induces epithelial to mesenchymal transition in culture. Oncogene *22*, 869–883.

Carro, M.S., Lim, W.K., Alvarez, M.J., Bollo, R.J., Zhao, X., Snyder, E.Y., Sulman, E.P., Anne, S.L., Doetsch, F., Colman, H., et al. (2010). The transcriptional network for mesenchymal transformation of brain tumours. Nature *463*, 318–325.

Chang, G.W., Hsiao, C.C., Peng, Y.M., Vieira Braga, F.A., Kragten, N.A., Remmerswaal, E.B., van de Garde, M.D., Straussberg, R., König, G.M., Kostenis, E., et al. (2016). The adhesion G protein-coupled receptor GPR56/ADGRG1 is an inhibitory receptor on human NK cells. Cell Rep. *15*, 1757–1770.

Chen, J.C., Alvarez, M.J., Talos, F., Dhruv, H., Rieckhof, G.E., Iyer, A., Diefes, K.L., Aldape, K., Berens, M., Shen, M.M., and Califano, A. (2014). Identification of causal genetic drivers of human disease through systems-level analysis of regulatory networks. Cell *159*, 402–414.

Cheng, W.Y., Kandel, J.J., Yamashiro, D.J., Canoll, P., and Anastassiou, D. (2012). A multi-cancer mesenchymal transition gene expression signature is associated with prolonged time to recurrence in glioblastoma. PLoS ONE *7*, e34705.

Creighton, C.J., Li, X., Landis, M., Dixon, J.M., Neumeister, V.M., Sjolund, A., Rimm, D.L., Wong, H., Rodriguez, A., Herschkowitz, J.I., et al. (2009). Residual breast cancers after conventional therapy display mesenchymal as well as tumor-initiating features. Proc. Natl. Acad. Sci. USA *106*, 13820–13825.

Dunn, G.P., Rinne, M.L., Wykosky, J., Genovese, G., Quayle, S.N., Dunn, I.F., Agarwalla, P.K., Chheda, M.G., Campos, B., Wang, A., et al. (2012). Emerging insights into the molecular and cellular basis of glioblastoma. Genes Dev. *26*, 756–784.

Edwards, L.A., Woolard, K., Son, M.J., Li, A., Lee, J., Ene, C., Mantey, S.A., Maric, D., Song, H., Belova, G., et al. (2011). Effect of brain- and tumor-derived connective tissue growth factor on glioma invasion. J. Natl. Cancer Inst. *103*, 1162–1178.

Fan, C., Prat, A., Parker, J.S., Liu, Y., Carey, L.A., Troester, M.A., and Perou, C.M. (2011). Building prognostic models for breast cancer patients using clinical variables and hundreds of gene expression signatures. BMC Med. Genomics *4*, 3.

Galli, R., Binda, E., Orfanelli, U., Cipelletti, B., Gritti, A., De Vitis, S., Fiocco, R., Foroni, C., Dimeco, F., and Vescovi, A. (2004). Isolation and characterization of tumorigenic, stem-like neural precursors from human glioblastoma. Cancer Res. *64*, 7011–7021.

Gerber, N.K., Goenka, A., Turcan, S., Reyngold, M., Makarov, V., Kannan, K., Beal, K., Omuro, A., Yamada, Y., Gutin, P., et al. (2014). Transcriptional diversity of long-term glioblastoma survivors. Neuro-oncol. *16*, 1186–1195.

Giera, S., Deng, Y., Luo, R., Ackerman, S.D., Mogha, A., Monk, K.R., Ying, Y., Jeong, S.J., Makinodan, M., Bialas, A.R., et al. (2015). The adhesion G protein-coupled receptor GPR56 is a cell-autonomous regulator of oligodendrocyte development. Nat. Commun. *6*, 6121.

Gilmore, T.D. (2006). Introduction to NF-kappaB: players, pathways, perspectives. Oncogene *25*, 6680–6684.

Gómez-Miragaya, J., Palafox, M., Paré, L., Yoldi, G., Ferrer, I., Vila, S., Galván, P., Pellegrini, P., Pérez-Montoyo, H., Igea, A., et al. (2017). Resistance to taxanes in triple-negative breast cancer associates with the dynamics of a CD49f+ tumor-initiating population. Stem Cell Reports *8*, 1392–1407.

Halliday, J., Helmy, K., Pattwell, S.S., Pitter, K.L., LaPlant, Q., Ozawa, T., and Holland, E.C. (2014). In vivo radiation response of proneural glioma characterized by protective p53 transcriptional program and proneural-mesenchymal shift. Proc. Natl. Acad. Sci. USA *111*, 5248–5253.

Iglesia, M.D., Vincent, B.G., Parker, J.S., Hoadley, K.A., Carey, L.A., Perou, C.M., and Serody, J.S. (2014). Prognostic B-cell signatures using mRNA-seq in patients with subtype-specific breast and ovarian cancer. Clin. Cancer Res. *20*, 3818–3829.

Iglesia, M.D., Parker, J.S., Hoadley, K.A., Serody, J.S., Perou, C.M., and Vincent, B.G. (2016). Genomic analysis of immune cell infiltrates across 11 tumor types. J. Natl. Cancer Inst. *108*, djw144.

Jeong, S.J., Luo, R., Li, S., Strokes, N., and Piao, X. (2012). Characterization of G protein-coupled receptor 56 protein expression in the mouse developing neocortex. J. Comp. Neurol. *520*, 2930–2940.

Keller, P.J., Arendt, L.M., Skibinski, A., Logvinenko, T., Klebba, I., Dong, S., Smith, A.E., Prat, A., Perou, C.M., Gilmore, H., et al. (2012). Defining the cellular precursors to human breast cancer. Proc. Natl. Acad. Sci. USA *109*, 2772–2777.

Kim, Y.W., Koul, D., Kim, S.H., Lucio-Eterovic, A.K., Freire, P.R., Yao, J., Wang, J., Almeida, J.S., Aldape, K., and Yung, W.K. (2013). Identification of prognostic gene signatures of glioblastoma: a study based on TCGA data analysis. Neuro-oncol. *15*, 829–839.

Kupp, R., Shtayer, L., Tien, A.C., Szeto, E., Sanai, N., Rowitch, D.H., and Mehta, S. (2016). Lineage-restricted OLIG2-RTK signaling governs the molecular subtype of glioma stem-like cells. Cell Rep. *16*, 2838–2845.

Langenhan, T., Aust, G., and Hamann, J. (2013). Sticky signaling–adhesion class G protein-coupled receptors take the stage. Sci. Signal. *6*, re3.

Lei, Q.Y., Zhang, H., Zhao, B., Zha, Z.Y., Bai, F., Pei, X.H., Zhao, S., Xiong, Y., and Guan, K.L. (2008). TAZ promotes cell proliferation and epithelial-mesenchymal transition and is inhibited by the hippo pathway. Mol. Cell. Biol. *28*, 2426–2436.

Lewis-Tuffin, L.J., Rodriguez, F., Giannini, C., Scheithauer, B., Necela, B.M., Sarkaria, J.N., and Anastasiadis, P.Z. (2010). Misregulated E-cadherin expression associated with an aggressive brain tumor phenotype. PLoS ONE *5*, e13665.

Li, S., Jin, Z., Koirala, S., Bu, L., Xu, L., Hynes, R.O., Walsh, C.A., Corfas, G., and Piao, X. (2008). GPR56 regulates pial basement membrane integrity and cortical lamination. J. Neurosci. *28*, 5817–5826.

Liu, C., Sage, J.C., Miller, M.R., Verhaak, R.G., Hippenmeyer, S., Vogel, H., Foreman, O., Bronson, R.T., Nishiyama, A., Luo, L., and Zong, H. (2011). Mosaic analysis with double markers reveals tumor cell of origin in glioma. Cell *146*, 209–221.

Lo, H.W., Hsu, S.C., Xia, W., Cao, X., Shih, J.Y., Wei, Y., Abbruzzese, J.L., Hortobagyi, G.N., and Hung, M.C. (2007). Epidermal growth factor receptor cooperates with signal transducer and activator of transcription 3 to induce epithelial-mesenchymal transition in cancer cells via up-regulation of TWIST gene expression. Cancer Res. *67*, 9066–9076.

Louis, D.N., Perry, A., Reifenberger, G., von Deimling, A., Figarella-Branger, D., Cavenee, W.K., Ohgaki, H., Wiestler, O.D., Kleihues, P., and Ellison, D.W. (2016). The 2016 World Health Organization classification of tumors of the central nervous system: a summary. Acta Neuropathol. *131*, 803–820.

Lu, F., Chen, Y., Zhao, C., Wang, H., He, D., Xu, L., Wang, J., He, X., Deng, Y., Lu, E.E., et al. (2016). Olig2-dependent reciprocal shift in PDGF and EGF receptor signaling regulates tumor phenotype and mitotic growth in malignant glioma. Cancer Cell *29*, 669–683.

Luo, R., Jeong, S.J., Jin, Z., Strokes, N., Li, S., and Piao, X. (2011). G protein-coupled receptor 56 and collagen III, a receptor-ligand pair, regulates cortical development and lamination. Proc. Natl. Acad. Sci. USA *108*, 12925–12930.

Mani, S.A., Guo, W., Liao, M.J., Eaton, E.N., Ayyanan, A., Zhou, A.Y., Brooks, M., Reinhard, F., Zhang, C.C., Shipitsin, M., et al. (2008). The epithelial-mesenchymal transition generates cells with properties of stem cells. Cell *133*, 704–715.

Mao, P., Joshi, K., Li, J., Kim, S.H., Li, P., Santana-Santos, L., Luthra, S., Chandran, U.R., Benos, P.V., Smith, L., et al. (2013). Mesenchymal glioma stem cells are maintained by activated glycolytic metabolism involving aldehyde dehydrogenase 1A3. Proc. Natl. Acad. Sci. USA *110*, 8644–8649.

Mir, S.E., De Witt Hamer, P.C., Krawczyk, P.M., Balaj, L., Claes, A., Niers, J.M., Van Tilborg, A.A., Zwinderman, A.H., Geerts, D., Kaspers, G.J., et al. (2010). In silico analysis of kinase expression identifies WEE1 as a gatekeeper against mitotic catastrophe in glioblastoma. Cancer Cell *18*, 244–257.

Noushmehr, H., Weisenberger, D.J., Diefes, K., Phillips, H.S., Pujara, K., Berman, B.P., Pan, F., Pelloski, C.E., Sulman, E.P., Bhat, K.P., et al. (2010). Identification of a CpG island methylator phenotype that defines a distinct subgroup of glioma. Cancer Cell *17*, 510–522.

Ozawa, T., Riester, M., Cheng, Y.K., Huse, J.T., Squatrito, M., Helmy, K., Charles, N., Michor, F., and Holland, E.C. (2014). Most human non-GCIMP glioblastoma subtypes evolve from a common proneural-like precursor glioma. Cancer Cell *26*, 288–300.

Parsons, D.W., Jones, S., Zhang, X., Lin, J.C., Leary, R.J., Angenendt, P., Mankoo, P., Carter, H., Siu, I.M., Gallia, G.L., et al. (2008). An integrated genomic analysis of human glioblastoma multiforme. Science *321*, 1807–1812.

Patel, A.P., Tirosh, I., Trombetta, J.J., Shalek, A.K., Gillespie, S.M., Wakimoto, H., Cahill, D.P., Nahed, B.V., Curry, W.T., Martuza, R.L., et al. (2014). Single-cell RNA-seq highlights intratumoral heterogeneity in primary glioblastoma. Science *344*, 1396–1401.

Phillips, H.S., Kharbanda, S., Chen, R., Forrest, W.F., Soriano, R.H., Wu, T.D., Misra, A., Nigro, J.M., Colman, H., Soroceanu, L., et al. (2006). Molecular subclasses of high-grade glioma predict prognosis, delineate a pattern of disease progression, and resemble stages in neurogenesis. Cancer Cell *9*, 157–173.

Piao, X., Hill, R.S., Bodell, A., Chang, B.S., Basel-Vanagaite, L., Straussberg, R., Dobyns, W.B., Qasrawi, B., Winter, R.M., Innes, A.M., et al. (2004). G protein-coupled receptor-dependent development of human frontal cortex. Science *303*, 2033–2036.

Piao, Y., Liang, J., Holmes, L., Henry, V., Sulman, E., and de Groot, J.F. (2013). Acquired resistance to anti-VEGF therapy in glioblastoma is associated with a mesenchymal transition. Clin. Cancer Res. *19*, 4392–4403.

Prasad, S., Ravindran, J., and Aggarwal, B.B. (2010). NF-kappaB and cancer: how intimate is this relationship. Mol. Cell. Biochem. *336*, 25–37.

Prat, A., Parker, J.S., Karginova, O., Fan, C., Livasy, C., Herschkowitz, J.I., He, X., and Perou, C.M. (2010). Phenotypic and molecular characterization of the claudin-low intrinsic subtype of breast cancer. Breast Cancer Res. *12*, R68.

Prat, A., Fan, C., Fernández, A., Hoadley, K.A., Martinello, R., Vidal, M., Viladot, M., Pineda, E., Arance, A., Muñoz, M., et al. (2015). Response and survival of breast cancer intrinsic subtypes following multi-agent neoadjuvant chemotherapy. BMC Med. *13*, 303.

Prater, M.D., Petit, V., Alasdair Russell, I., Giraddi, R.R., Shehata, M., Menon, S., Schulte, R., Kalajzic, I., Rath, N., Olson, M.F., et al. (2014). Mammary stem cells have myoepithelial cell properties. Nat. Cell Biol. *16*, 942–950.

Rody, A., Holtrich, U., Pusztai, L., Liedtke, C., Gaetje, R., Ruckhaeberle, E., Solbach, C., Hanker, L., Ahr, A., Metzler, D., et al. (2009). T-cell metagene predicts a favorable prognosis in estrogen receptor-negative and HER2-positive breast cancers. Breast Cancer Res. *11*, R15.

Segerman, A., Niklasson, M., Haglund, C., Bergström, T., Jarvius, M., Xie, Y., Westermark, A., Sönmez, D., Hermansson, A., Kastemar, M., et al. (2016). Clonal variation in drug and radiation response among glioma-initiating cells is linked to proneural-mesenchymal transition. Cell Rep. *17*, 2994–3009.

Siebzehnrubl, F.A., Silver, D.J., Tugertimur, B., Deleyrolle, L.P., Siebzehnrubl, D., Sarkisian, M.R., Devers, K.G., Yachnis, A.T., Kupper, M.D., Neal, D., et al. (2013). The ZEB1 pathway links glioblastoma initiation, invasion and chemoresistance. EMBO Mol. Med. *5*, 1196–1212.

Subramanian, A., Tamayo, P., Mootha, V.K., Mukherjee, S., Ebert, B.L., Gillette, M.A., Paulovich, A., Pomeroy, S.L., Golub, T.R., Lander, E.S., and Mesirov, J.P. (2005). Gene set enrichment analysis: a knowledge-based approach for interpreting genome-wide expression profiles. Proc. Natl. Acad. Sci. USA *102*, 15545–15550.

Taube, J.H., Herschkowitz, J.I., Komurov, K., Zhou, A.Y., Gupta, S., Yang, J., Hartwell, K., Onder, T.T., Gupta, P.B., Evans, K.W., et al. (2010). Core epithelial-to-mesenchymal transition interactome gene-expression signature is

associated with claudin-low and metaplastic breast cancer subtypes. Proc. Natl. Acad. Sci. USA *107*, 15449–15454.

Thiery, J.P., Acloque, H., Huang, R.Y., and Nieto, M.A. (2009). Epithelial-mesenchymal transitions in development and disease. Cell *139*, 871–890.

Tusher, V.G., Tibshirani, R., and Chu, G. (2001). Significance analysis of microarrays applied to the ionizing radiation response. Proc. Natl. Acad. Sci. USA *98*, 5116–5121.

Van Laere, S.J., Ueno, N.T., Finetti, P., Vermeulen, P., Lucci, A., Robertson, F.M., Marsan, M., Iwamoto, T., Krishnamurthy, S., Masuda, H., et al. (2013). Uncovering the molecular secrets of inflammatory breast cancer biology: an integrated analysis of three distinct affymetrix gene expression datasets. Clin. Cancer Res. *19*, 4685–4696.

Verhaak, R.G., Hoadley, K.A., Purdom, E., Wang, V., Qi, Y., Wilkerson, M.D., Miller, C.R., Ding, L., Golub, T., Mesirov, J.P., et al.; Cancer Genome Atlas Research Network (2010). Integrated genomic analysis identifies clinically relevant subtypes of glioblastoma characterized by abnormalities in PDGFRA, IDH1, EGFR, and NF1. Cancer Cell *17*, 98–110.

Wang, J., Cazzato, E., Ladewig, E., Frattini, V., Rosenbloom, D.I., Zairis, S., Abate, F., Liu, Z., Elliott, O., Shin, Y.J., et al. (2016). Clonal evolution of glioblastoma under therapy. Nat. Genet. *48*, 768–776.

Wang, Q., Hu, B., Hu, X., Kim, H., Squatrito, M., Scarpace, L., deCarvalho, A.C., Lyu, S., Li, P., Li, Y., et al. (2017). Tumor evolution of glioma-intrinsic gene expression subtypes associates with immunological changes in the microenvironment. Cancer Cell *32*, 42–56.e6.

Wirapati, P., Sotiriou, C., Kunkel, S., Farmer, P., Pradervand, S., Haibe-Kains, B., Desmedt, C., Ignatiadis, M., Sengstag, T., Schütz, F., et al. (2008). Meta-analysis of gene expression profiles in breast cancer: toward a unified understanding of breast cancer subtyping and prognosis signatures. Breast Cancer Res. *10*, R65.

Xie, Y., Bergström, T., Jiang, Y., Johansson, P., Marinescu, V.D., Lindberg, N., Segerman, A., Wicher, G., Niklasson, M., Baskaran, S., et al. (2015). The human glioblastoma cell culture resource: validated cell models representing all molecular subtypes. EBioMedicine *2*, 1351–1363.

Xiong, H., Hong, J., Du, W., Lin, Y.W., Ren, L.L., Wang, Y.C., Su, W.Y., Wang, J.L., Cui, Y., Wang, Z.H., and Fang, J.Y. (2012). Roles of STAT3 and ZEB1 proteins in E-cadherin down-regulation and human colorectal cancer epithelial-mesenchymal transition. J. Biol. Chem. *287*, 5819–5832.

Xu, L., Begum, S., Hearn, J.D., and Hynes, R.O. (2006). GPR56, an atypical G protein-coupled receptor, binds tissue transglutaminase, TG2, and inhibits melanoma tumor growth and metastasis. Proc. Natl. Acad. Sci. USA *103*, 9023–9028.

Xu, L., Begum, S., Barry, M., Crowley, D., Yang, L., Bronson, R.T., and Hynes, R.O. (2010). GPR56 plays varying roles in endogenous cancer progression. Clin. Exp. Metastasis *27*, 241–249.

Yan, H., Parsons, D.W., Jin, G., McLendon, R., Rasheed, B.A., Yuan, W., Kos, I., Batinic-Haberle, I., Jones, S., Riggins, G.J., et al. (2009). IDH1 and IDH2 mutations in gliomas. N. Engl. J. Med. *360*, 765–773.